A&A 390, 47–58 (2002)
DOI: 10.1051/0004-6361:20020709

Astronomy & Astrophysics

H_γ and H_δ absorption lines and the Initial Mass Function in extragalactic star forming regions

I. Data

A. Sinanian[1], D. Kunth[2], J. Lequeux[3], G. Comte[4], and A. Petrosian[1]

[1] Byurakan Astrophysical Observatory and Isaac Newton Institute of Chile, Armenian Branch, 378443 Byurakan, Armenia
[2] Institut d'Astrophysique de Paris, CNRS, 98-bis Boulevard Arago, 75014 Paris, France
[3] Observatoire de Paris, 61 avenue de l'Observatoire, 75014 Paris, France
[4] Observatoire Astronomique de Marseille-Provence and Laboratoire d'Astrophysique de Marseille, 2 place Le Verrier, 13248 Marseille, France

Received 30 January 2002 / Accepted 15 May 2002

Abstract. High-dispersion, long-slit spectroscopic observations of 13 extragalactic star–forming regions were obtained for two Blue Compact Dwarf galaxies (IZw18, IZw36) and for bright star–formation regions in the spiral galaxies M 101 and M 51 and in the irregular starburst galaxies Mrk 171 and NGC 4449. The H_γ and/or H_δ absorption lines have been observed in 11 star forming regions and will be used to constrain the Initial Mass Function and age of the young stellar populations. In this paper we present the results of the observations and the measurements of the absorption and emission lines. The astrophysical discussion is deferred to a forthcoming paper.

Key words. galaxies: evolution – galaxies: stellar content – ISM: H II regions

1. Introduction

The formation of stars in extragalactic starbursts is still far from being fully understood. One problem is that of the Initial Mass Function (IMF) of massive stars. Is the IMF everywhere the same, or does it depend on environment, metallicity and other parameters? In order to answer this question, determinations of the IMF in as many active star formation regions as possible with a variety of conditions are required. Unfortunately the IMF can be determined directly by photometry of individual stars only in very nearby galaxies. In the main star formation region of the Large Magellanic Cloud, 30 Doradus, the IMF of the central cluster R 136 is close to the classical Salpeter one from 3 to >100 $M_\odot$, with some flattening below 2 $M_\odot$ (Sirianni et al. 2000). Similar, although less precise, results exist for other young clusters or associations of the Magellanic Clouds (Parker et al. 1992; Oey & Massey 1995; Holtzman et al. 1997), suggesting that the IMF is similar in all these objects. But little has been done on more distant star formation regions.

Another problem is the history of formation of stars in these starbursts. We know even less on this point. As an example of the information we have at present, there are evidences for approximately continuous star formation in the last 5 Myr in R 136 (Massey & Hunter 1998), while the presence of red supergiants in the surroundings (Hyland et al. 1992 and references herein), demonstrates that another burst of star formation has taken place some 20 million years ago.

For more distant galaxies of the Local group, observations of individual stars are considerably more difficult although interesting results have been obtained with the Hubble Space Telescope on the upper part of the IMF. Some results have even been obtained at larger distances, but it becomes almost impossible to resolve the central parts of stars clusters. Then the only way to obtain information on the IMF is to compare observations with the predictions of evolutionary population synthesis models. This has been done for example by Lequeux et al. (1981), Arnault et al. (1989), Mas–Hesse & Kunth (1991, 1999), Schaerer & Vacca (1998), Kewley et al. (2001), Moy et al. (2001), Stasinska et al. (2001). The Balmer lines of hydrogen are particularly interesting for population synthesis of very young clusters. The emission lines from the surrounding H II region give the flux in the Lyman continuum hence information on O stars, while the absorption lines resulting from the stellar photospheres are strongest for A stars and give information on a broader portion of the mass spectrum of stars. Another advantage of Balmer lines is that they are relatively insensitive to metallicity. Unfortunately the emission and absorption lines of young clusters are superimposed. Low order Balmer absorption lines are more strongly affected by emission lines than higher order Balmer ones since the equivalent width of the emission decreases at higher order while for the absorption it remains

Send offprint requests to: D. Kunth, e-mail: kunth@iap.fr

more or less constant. In low-resolution spectral observations of extragalactic starburst regions, the absorption component contaminates the (stronger) emission component and causes biases in the determination of the intensity of emission lines. The absorption and emission components can only be separated using a spectrograph with high spectral resolution and good Point Spread Function (PSF), and with a good signal to noise ratio. This explains why little has been done on this topic. Absorption Balmer lines have almost exclusively been used in population synthesis studies of relatively old stellar populations for which there is no emission component (see e.g. Rose 1985, 1994; Jones & Worthey 1995; Worthey 1996; Worthey & Ottaviani 1997) evolutionary synthesis mdels have used for the young stellar populations as well (see e.g. Gonzalez-Delgado & Leitherer 1999; Gonzalez-Delgado et al. 1999; Boker et al. 2001; Bresolin & Kennicutt 2002).

The aim of the present study is to use the equivalent widths of the emission and absorption components of the H_γ and H_δ lines to constrain the properties of the stellar population in star–forming regions of spiral, irregular and blue compact dwarf galaxies. For this purpose 13 H II regions in 6 galaxies were observed with high spatial and spectral resolution. These H II regions were chosen because they are bright and relatively nearby so that our results can be compared to those of direct observations of stellar populations in the same objects and can serve as templates for future studies of more distant galaxies. In the present paper we describe the observations and the data reductions (Sect. 2), then the determination of the emission and absorption equivalent widths of the H_γ and H_δ lines (Sect. 3). For a consistency check the intensity of the H_β emission line will be calculated from those of the H_γ and H_δ lines and compared with direct measurements by other authors. These data will be used for setting constraints on the IMF and star formation history in a further paper. This will use spectral syntheses based on the models of Mas-Hesse (Mas-Hesse & Cerviño 1994). For absorption lines we will use a library of stellar spectra obtained especially for this purpose with the same instrument as the present one (Cananzi et al. 1993).

2. The data

2.1. The observations

Long slit spectra of HII regions in two Blue Compact Dwarf, two Spiral and two Irregular galaxies were obtained at the OHP 193 cm telescope, during a run of six nights (31.03.95 - 5.04.95). In Table 1, for all the objects of our sample, the name and morphological type of the galaxies, and the dates, position angles and exposure times of the observations are listed. The instrument used was the CARELEC spectrograph (Lemaître et al. 1990). Spectra have been taken in the blue spectral region, between 4000 Å and 4500 Å with a dispersion of 33 Å/mm (resolution R = 2000). The slit width was 2.5″, to allow a correct comparison of the spectrum with the spectra of a number of stars of different types, which were taken previously for calibrating the Balmer absorption line equivalent widths (Cananzi et al. 1993).

Table 1. Log of observations.

Object	Morph. type	Date	Pos. angle (deg)	Exp. time (s)
IZw18	BCDG	01.04.95	144	2400
		01.04.95	144	2400
		02.04.95	145	3000
		02.04.95	145	3000
		02.04.95	145	4000
		02.04.95	145	4000
IZw36	BCDG	04.04.95	274	3000
		04.04.95	274	4000
		04.04.95	274	5000
		04.04.95	274	1800
		04.04.95	274	1800
NGC 5461	H II	04.04.95	30	3000
	Region	04.04.95	30	5000
	in Spiral	05.04.95	210	5000
	Galaxy	05.04.95	210	3600
	M 101	05.04.95	210	3600
NGC 5471	H II	31.03.95	315	3000
	Region	31.03.95	315	3000
	in Spiral	03.04.95	315	3600
	Galaxy	03.04.95	315	3000
	M 101	03.04.95	315	3000
		03.04.95	315	2400
Mrk 171	Irregular	31.03.95	266	3000
	Galaxy	31.03.95	266	3000
		31.03.95	266	3000
		31.03.95	266	3000
		03.04.95	266	2400
		03.04.95	266	2400
M 51	Spiral	02.04.95	164	3000
	Galaxy	02.04.95	164	5000
		03.04.95	164	3000
		03.04.95	164	3600
		03.04.95	164	1800
NGC 4449	Irregular	01.04.95	197	2400
	Galaxy	01.04.95	197	2400
		01.04.95	197	2400
		01.04.95	197	2400
		01.04.95	197	3000
		01.04.95	197	3000

2.2. Data reduction

All spectra have been reduced with the IRAF package using standard procedures, which included flat field correction, bias subtraction, distortion correction, wavelength calibration, sky subtraction and conversion to absolute fluxes. The wavelength calibration was done with an IRAF procedure relying on the

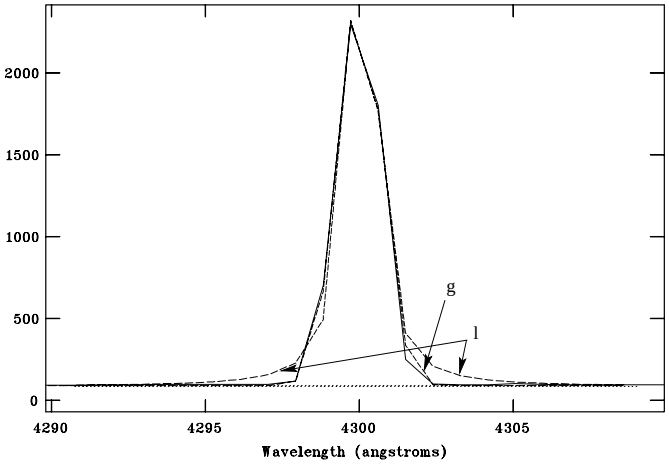

Fig. 1. The fits of argon line profile with a Lorenzian (l) and a Gaussian (g).

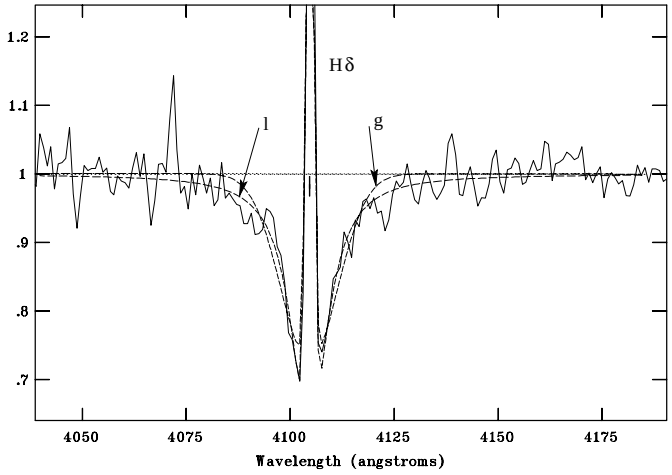

Fig. 2. The fits of H_δ line of NGC 4449 with Lorenzian (l) and Gaussian (g) profiles.

comparison argon spectrum. For checking distortion, measurements have been done along calibration lines: the rms error derived varies between 0.005 Å and 0.05 Å. In order to test the stability of the instrument, argon spectra, obtained during the same night were compared. The largest shifts are about 0.06 Å. The spectra of standard stars observed several times during each night have been used in order to flux calibrate the spectra. The error in the flux calibration is estimated to be about 6%.

Background subtraction was done using those parts of the spectra of the galaxies, which were not part of the star–forming region itself but were very close to it. This approach allows to remove the sky radiation as well as the background radiation of the galactic disk or arm. The light continuum of the host galaxy affects the calculated equivalent width to less then 1% on most cases. Final one-dimensional spectra of star forming regions have been derived from the two-dimensional ones by adding the intensity across the dispersion. The continuum along the dispersion has been fitted by the function *Spline3*, using different parameters before choosing the best fit.

2.3. Measurement of equivalent widths

The first problem we are dealing with in the measurements of the equivalent widths is the separation of the absorption and emission lines. For separating the emission and absorption lines one should take high-resolution spectra with a spectrograph whose PSF is well known and is without wings. To check the wings we have fitted in different ways Ar lines in the calibration spectra. The fits have been done interactively through the IRAF task *SPLOT* (Fig. 1).

Gaussian and Lorenzian profiles were used for fitting and it was found that the Gaussian fit is more acceptable than the Lorenzian. This justifies the use of a Gaussian for fitting the emission components of H_γ and H_δ lines. The hydrogen lines H_γ and H_δ have been fitted interactively by Gaussian fits through the IRAF task *SPLOT*. This procedure allows to fit emission as well as absorption components of the lines. The advantage of this fitting is that the absorption components are fitted using the wings and the emission components are fitted using their central parts. Moreover, using the same IRAF task *SPLOT* the Lorenzian profiles were used for the fitting.

The Lorenzian fits well the central parts of the line's profiles, but not well the wings. The Gaussian fits perfectly both the central part of the line profiles and the wings (Fig. 2). For this reason, hydrogen lines equivalent widths were measured by Gaussian fitting. For each line the combination of two Gaussians, one for the absorption and one for the emission, were used. For a few lines, which have a low S/N, equivalent widths were measured by integration. Before this integration, the absorption and the emission components were simply separated manually. When the comparison is possible, we find that the equivalent widths measured by integration are smaller ($\approx$0.6 Å) than the equivalent widths measured by Gaussian fitting. This comparison proves that the Gaussian fits involve all the information about real absorption. In Figs. 3–14 we show all the spectra of observed star forming regions: absolute intensity spectra; spectra with the continuum normalized to 1; H_γ and H_δ lines fitted by Gaussians. The IRAF procedure measuring the equivalent widths of "complex" profiles is based on a polynomial interpolation between the two intersection points of the line profile and the continuum. The level of the continuum strongly affects the measurement of the equivalent widths. To get an idea on the measurement errors, we have compared equivalent widths obtained using the same set of fitting parameters and different levels of the continuum of the same spectra. Because of the different S/N ratios, error estimation has been done for all the spectra and for each line individually. In Table 2 the measured equivalent widths of hydrogen lines H_γ and H_δ for absorption as well as for emission components and also S/N ratio of the continuum at 4250 Å are presented. Measured equivalent widths are in the good agreement with the values from the literature (Shields & Searle 1978; McCall et al. 1985; Petrosian & Burenkov 1993).

Table 2. Observed line equivalent widths in absorption and in emission.

Object	$EW(H_\gamma)$ab Å	$EW(H_\delta)$ab Å	$EW(H_\gamma)$em Å	$EW(H_\delta)$em Å	S/N continuum (4250 Å)
IZw 18	2.62 ± 0.64	2.97 ± 0.71	35.61 ± 6.34	14.15 ± 2.91	16
IZw 36	1.88 ± 0.42	1.98 ± 0.44	82.04 ± 9.72	39.38 ± 6.52	21
NGC 5461	−−	−−	78.68 ± 8.83	35.35 ± 5.44	21
NGC 5471	−−	1.65 ± 0.21	59.50 ± 4.71	27.67 ± 2.13	45
Mrk 171(A)	2.32 ± 0.25	3.36 ± 0.31	7.57 ± 0.57	3.54 ± 0.25	49
Mrk 171(B)	3.10 ± 0.32	4.12 ± 0.43	12.08 ± 1.17	5.06 ± 0.48	25
M 51(CCM71)	1.70 ± 0.51	1.87 ± 0.56	9.38 ± 2.82	4.45 ± 1.36	19
M 51(CCM72)	−−	−−	24.2 ± 4.91	12.5 ± 2.24	15
NGC 4449(A)[1]	4.60 ± 0.31	4.94 ± 0.33	2.15 ± 0.12	0.63 ± 0.11	30
NGC 4449(B)[2]	4.58 ± 0.31	5.24 ± 0.35	3.81 ± 0.20	1.63 ± 0.17	45
NGC 4449(C)[3]	4.20 ± 0.27	4.62 ± 0.30	6.17 ± 0.36	2.75 ± 0.19	36
NGC 4449(D)[4]	2.66 ± 0.23	3.03 ± 0.27	5.87 ± 0.48	2.45 ± 0.27	33
NGC 4449(E)[5]	−−	2.06 ± 0.38	78.35 ± 8.5	35.47 ± 5.4	30

[1] Eastern part of # 18 region of Hill et al. (1998) and # 27 region of Hodge & Kennicutt (1983);
[2]# 16 region of Hill et al. (1998) and # 23 region of Hodge & Kennicutt (1983);
[3]# 14 region of Hill et al. (1998) and # 20 region of Hodge & Kennicutt (1983);
[4]# 7 region of Hill et al. (1998);
[5]# 6 region of Hill et al. (1998), #11 region of Hodge & Kennicutt (1983) and CM 39 (Crillon & Monnet 1969).

2.4. Equivalent width of the H_β emission line

In the forthcoming paper results of the stellar population modelling with various parameters of IMF will be presented. Age estimation is one of the important aspects of stellar population modelling, and the equivalent width of the H_β emission line is a well-known tool for age determination (Copetti et al. 1985; Mas-Hesse & Kunth 1991; Mas-Hesse & Cerviño 1994). Since we did not observe the H_β line, we estimated its equivalent width from the H_γ and H_δ lines equivalent widths in emission and the values of the continuum. Using case B Balmer recombination decrement for $T_e = 10^4$ K and $n_e = 10^4$ cm^{-3} (Brocklehurst 1971) and the standard Whitford (1958) reddening curve we have estimated the reddening parameter c_{H_β} (Table 3) hence calculated the conrresponding equivalent width of H_β. The reddening parameter c_{H_β} is usually calculated from the H_α and H_β hydrogen lines, but as both lines have not been observed H_γ and H_δ lines were used instead to estimate the c_{H_β} parameter.

The values of equivalent widths we obtained are compared in Table 3 with values coming from direct observations reported in the literature. While collecting the data of equivalent widths we took the values, which were observed using slit width closer to ours. The error estimation was done on the bases of derived errors of the equivalent widths for H_γ and H_δ lines, as well as on the bases of the errors of the continuum. In general, our calculated values of H_β emission line equivalent widths are in good agreement with data from literature. The twice higher value of H_β equivalent width for the region "E" in NGC 4449 has the following reason: the slit, in our case, crosses the central high density star forming part of the region for which the determination of the equivalent width was done, while the determination taken from Hill et al. (1998), was done for a broader area which includes the central star forming part as well as the outer diffuse environment of the region.

Table 3. Calculated equivalent widths of H_β line compared with published data for the observed sample.

Object	$EW(H_\beta)$em. $(_{\text{calculated}})$	$EW(H_\beta)$em. $(_{\text{literature}})$	Ref.	c_{H_β}
IZw18	109.9 ± 32.0	104	1	0.96
IZw36	203.1 ± 39.5	224	1	0.12
NGC 5461	215.5 ± 40.1	195	2	0.11
NGC 5471	151.4 ± 15.1	129	2	0.38
Mrk 171(A)	19.2 ± 2.0	20	3	0.39
Mrk 171(B)	34.2 ± 5.5	35	3	1.26
M 51(CCM71)	21.3 ± 9.5	22	4	0.03
M 51(CCM72)	54.6 ± 15.7	64	4	0.14
NGC 4449(A)	13.8 ± 2.1	15	5	2.16
NGC 4449(B)	12.1 ± 1.5	11	5	0.75
NGC 4449(C)	18.7 ± 2.1	15	5	0.09
NGC 4449(D)	26.3 ± 4.7	28	5	0.26
NGC 4449(E)	211.4 ± 38.2	101	5	0.06

References: 1: Izotov et al. (1997); 2: Torres-Peimbert et al. (1989); 3: Mazzarella & Boroson (1993); 4: Díaz et al. (1991); 5: Hill et al. (1998).

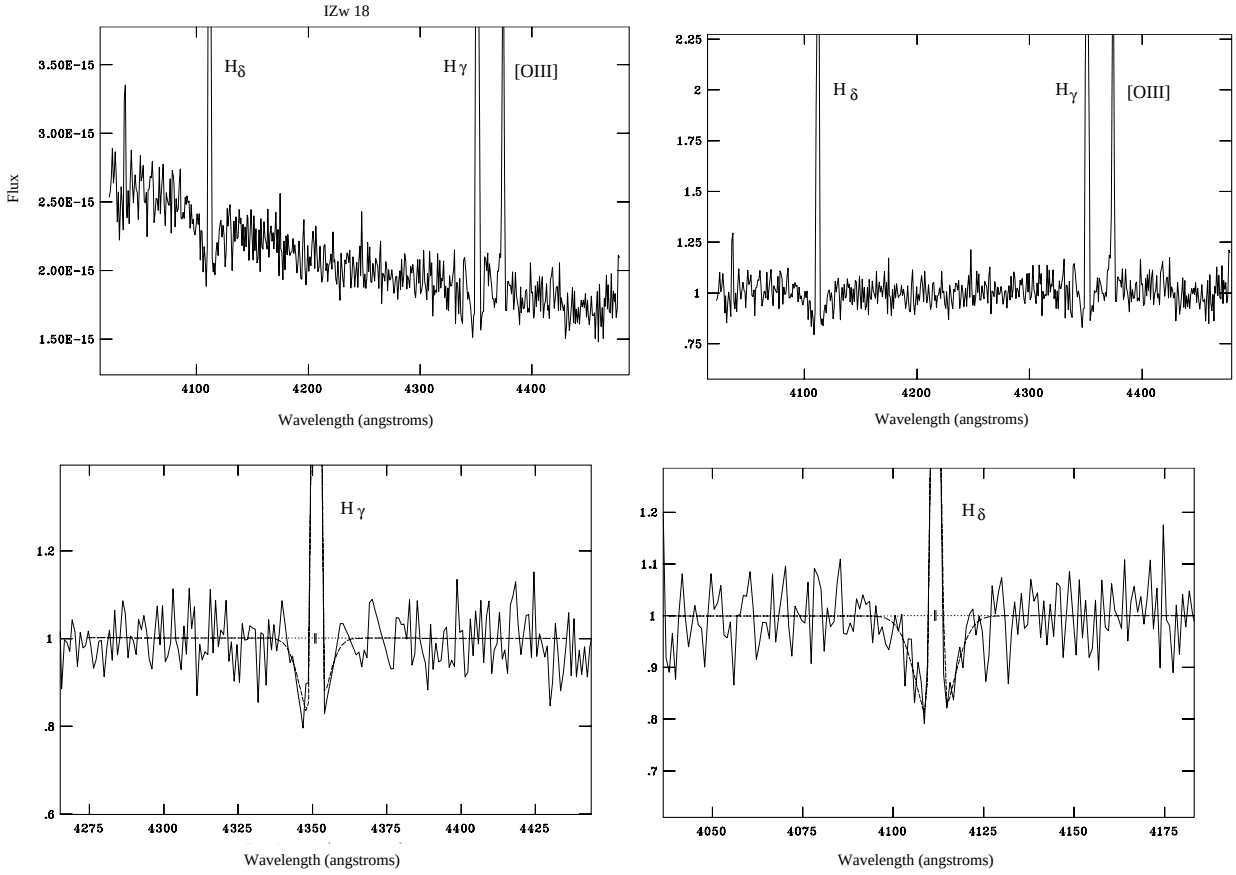

Fig. 3. IZw18: *(top; from left to right)* absolute flux corrected spectrum; normalized spectrum; *(bottom; from left to right)* H_γ and H_δ lines with the Gaussian fit.

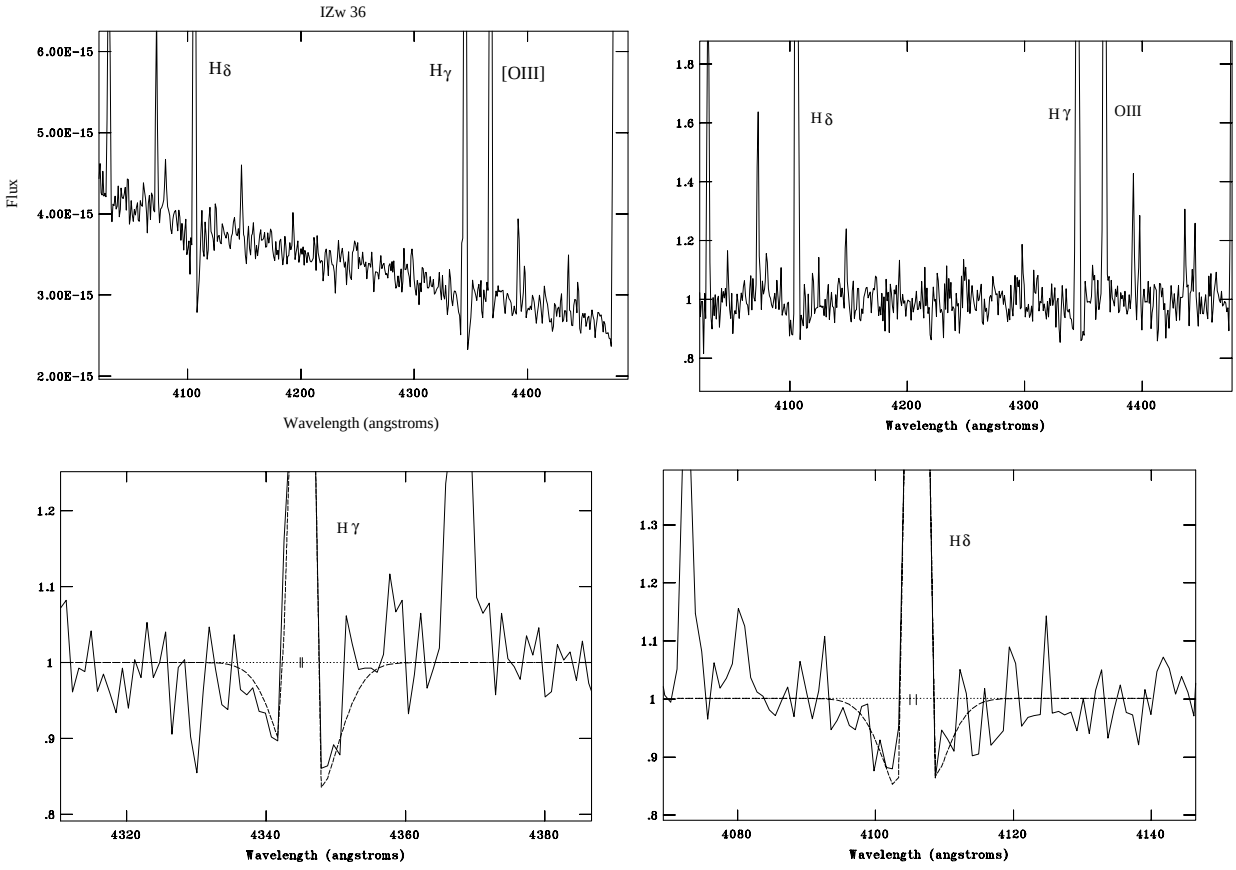

Fig. 4. IZw36: same legend as for Fig. 3.

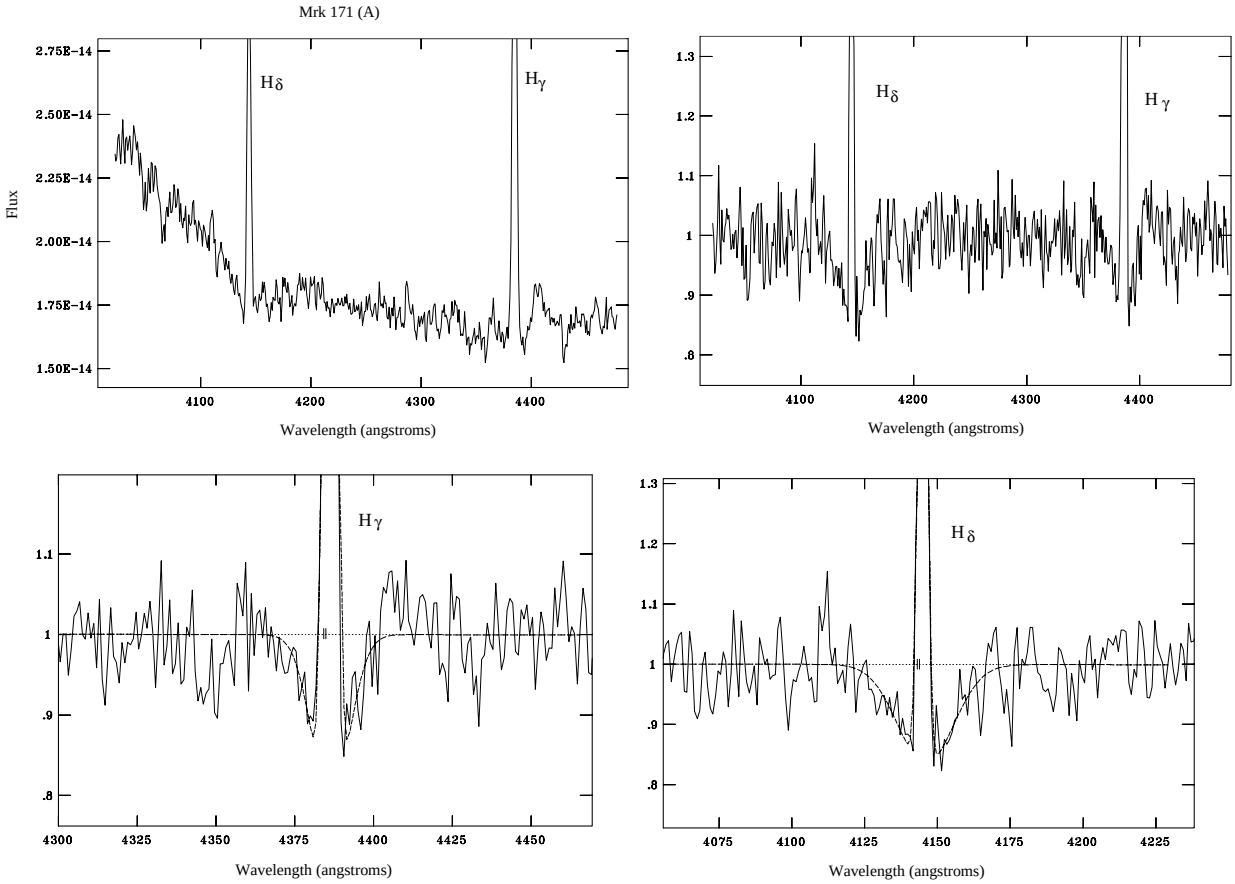

Fig. 5. Mrk 171 (A): same legend as for Fig. 3.

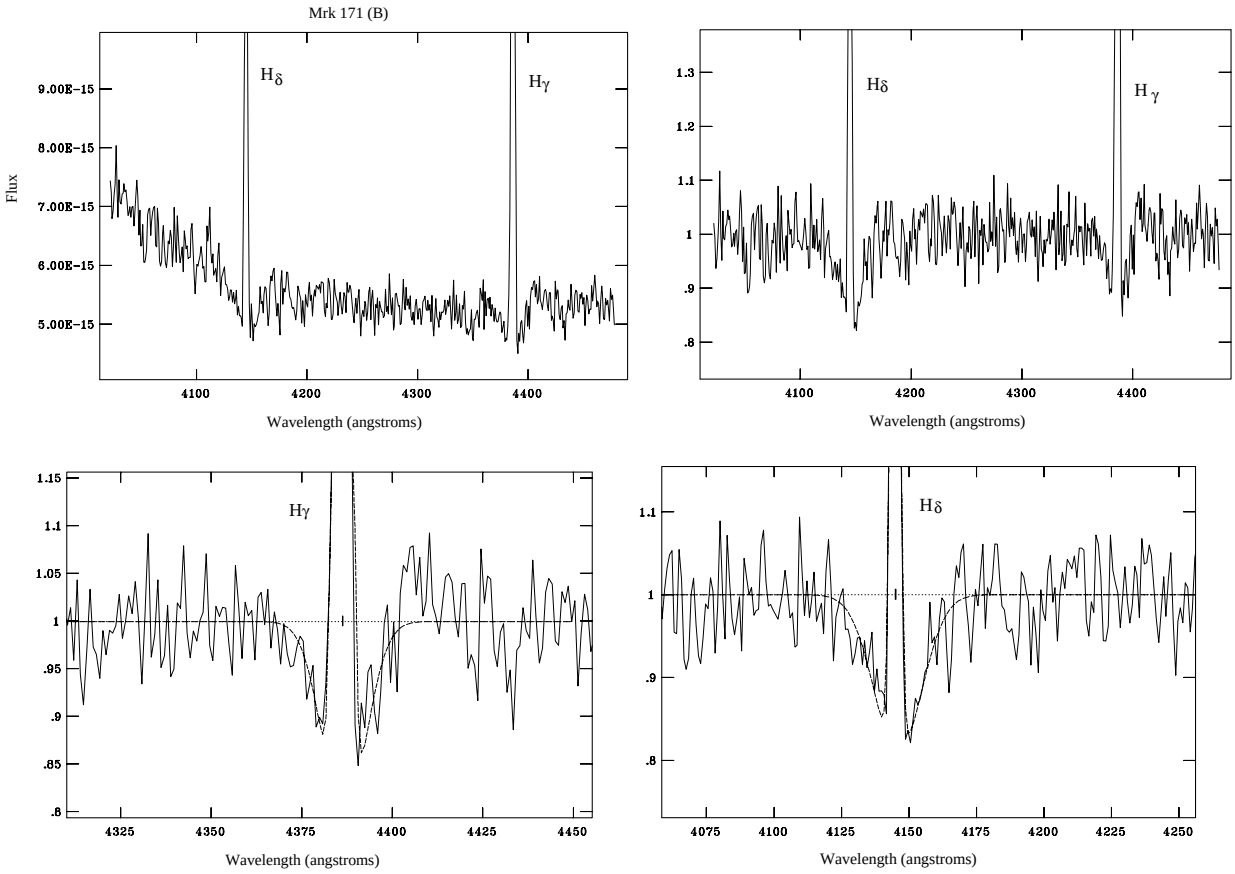

Fig. 6. Mrk 171 (B): same legend as for Fig. 3.

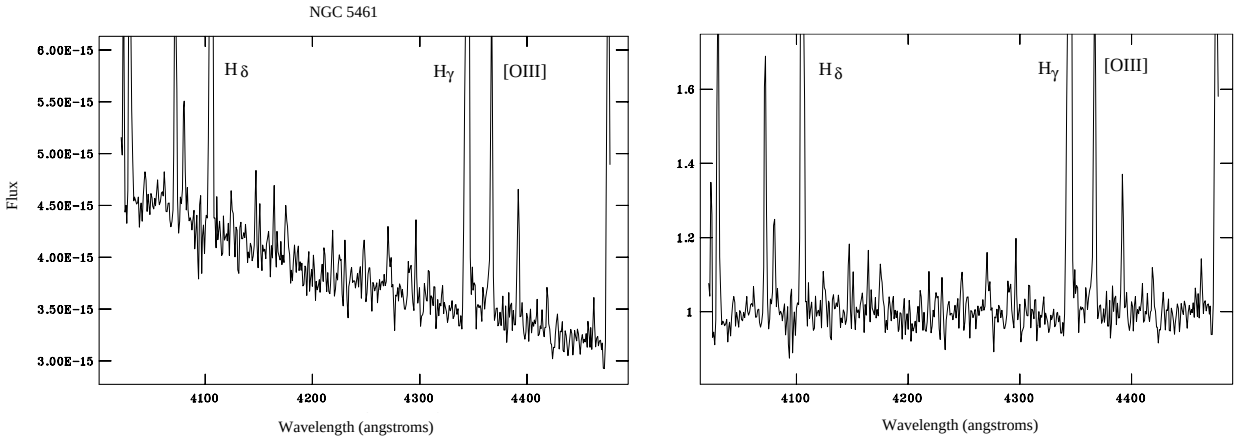

Fig. 7. NGC 5461: *(from left to right)* absolute flux corrected spectrum; normalized spectrum. No H_γ and H_δ absorption component is visible.

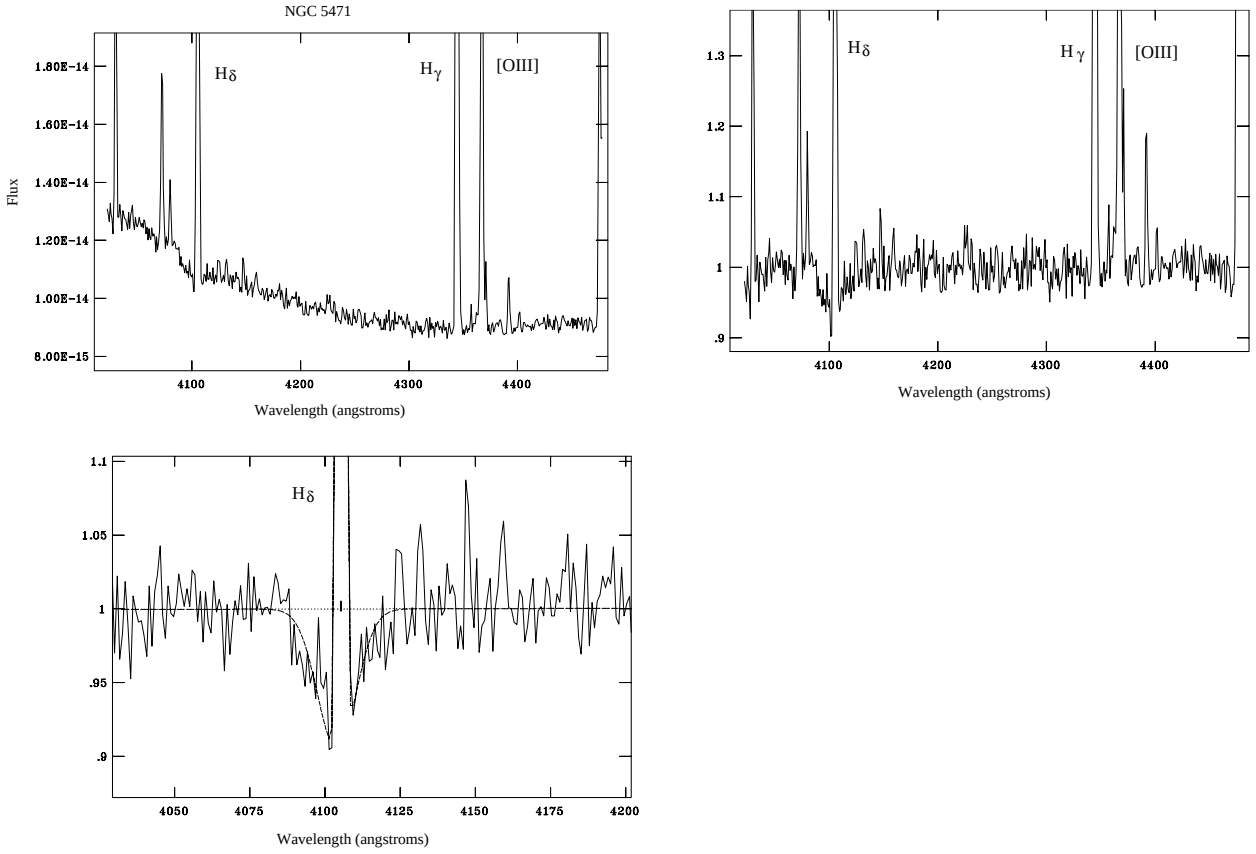

Fig. 8. NGC 5471: *(top; from left to right)* absolute flux corrected spectrum; normalized spectrum; *(bottom)* H_δ line with the Gaussian fit.

2.5. Comments of individual objects

In the case of three nearby galaxies (NGC 4449; M 51; Mrk 171) the slit covers several star forming regions in the host objects. Some of these star forming regions were identified and observed previously. Below for each of these galaxies short description as well as cross identification of observed star forming regions are presented.

NGC 4449: The Magellanic irregular galaxy NGC 4449 offers an important opportunity to study the processes by which star formation is sustained and propagated in irregular galaxies. The first studies of HII regions in NGC 4449 have been done by Crillon & Monnet (1969) and by Hodge (1969). Later more detailed investigations have been made by several authors (Hodge & Kennicutt 1983; Hill et al. 1998). In Fig. 15 our slit position on the NGC 4449 is shown. The slit covers five star forming regions in the galaxy. These star forming regions are marked by the letters (A, B, C, D and E). Cross identifications with previous determinations are presented in Table 2.

M 51: M 51 is a high metallicity face-on Sc galaxy with a well-defined spiral structure. In Fig. 16 our slit position for M 51 is shown. Two star forming regions were covered by slit, which are marked by the letters “A” and “B”. They correspond respectively to CCM71 and CCM72 of Carranza et al. (1969).

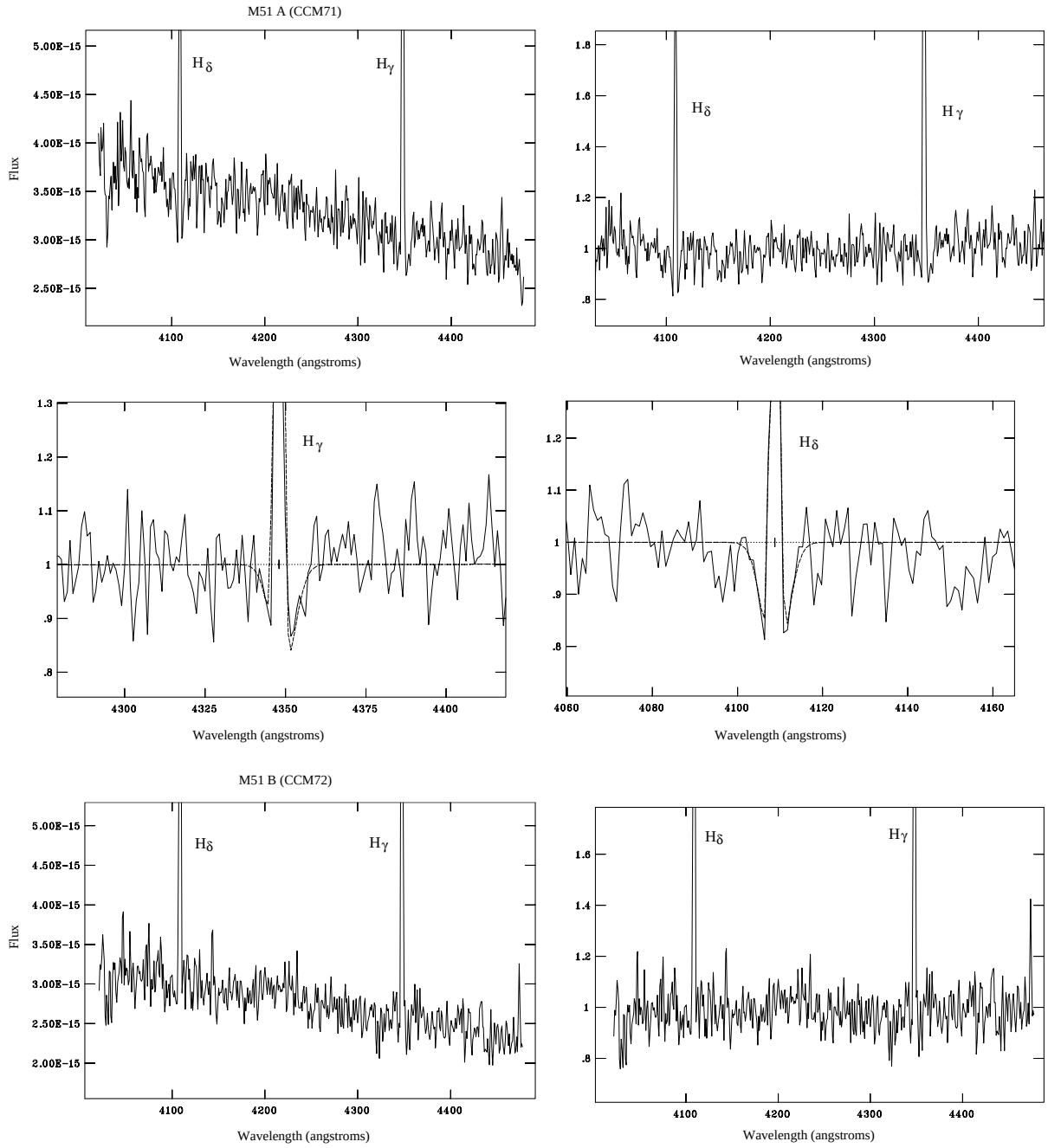

Fig. 9. M 51: for CCM71, *(top; from left to right)* absolute flux corrected spectrum; normalized spectrum; *(middle)* respectively H_γ and H_δ lines with the Gaussian fit. For the CCM72, *(bottom)* absolute flux corrected spectrum; normalized spectrum. No absorption component is visible.

Both "A" and "B" regions have strong emission in H_γ and H_δ lines. For the region "B" emission fills fully the absorption and it was impossible to measure its absorption component.

Mrk 171: Mrk 171 is a good example of an interacting system. The main interest of this object is that it is one of the most extreme cases known of an extended burst of star formation (Augarde & Lequeux 1985). In Fig. 17 our slit position for Mrk 171 is shown. Two "A" and "B" regions were covered by the slit. Comparison with previous long slit observations of the object by Mazzarella & Boroson (1993) shows that the star–forming region marked as "A" corresponds to the sum of the "c" and "g" regions and "B" corresponds to the sum of the "d", "e" and "f" regions of Mazzarella & Boroson (1993).

3. Conclusions

In this paper based on high resolution blue spectra of 13 HII regions in the galaxies with different morphologies (BCDGs, Irregular and Spiral galaxies), the Balmer lines H_γ and H_δ, with complex profiles, have been studied. For all 13 star forming regions equivalent widths of H_γ and H_δ emission lines have been measured and are presented. In 11 HII regions profiles of H_γ and/or H_δ lines exhibit absorption and emission components. For these objects the equivalent widths of H_γ and H_δ absorption as well as emission lines have been measured and are presented. From the measured H_γ and H_δ emission lines, the equivalent widths of the H_β emission line have been calculated. The results will be used in a forthcoming paper for modelling

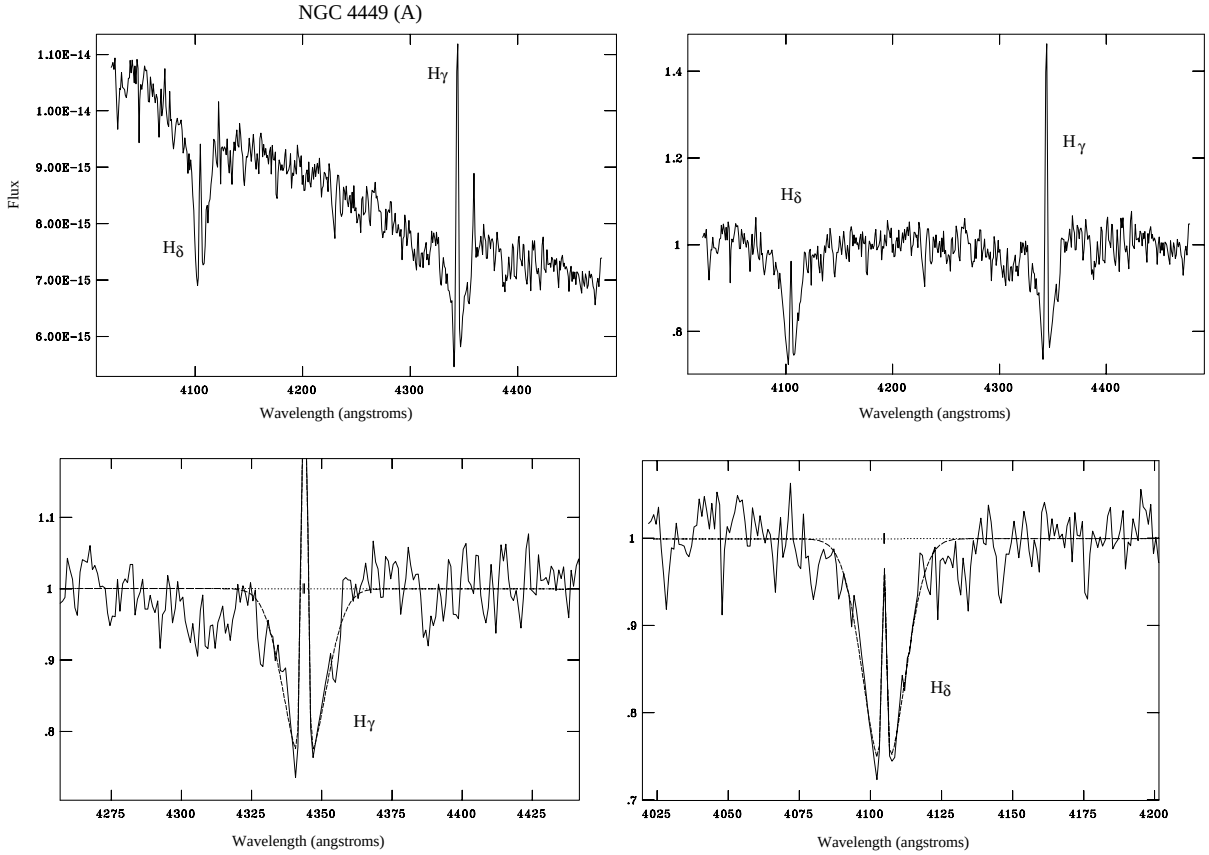

Fig. 10. NGC 4449 (A): *(top; from left to right)* absolute flux corrected spectrum; normalized spectrum; *(bottom)* respectively H_γ and H_δ lines with the Gaussian fit.

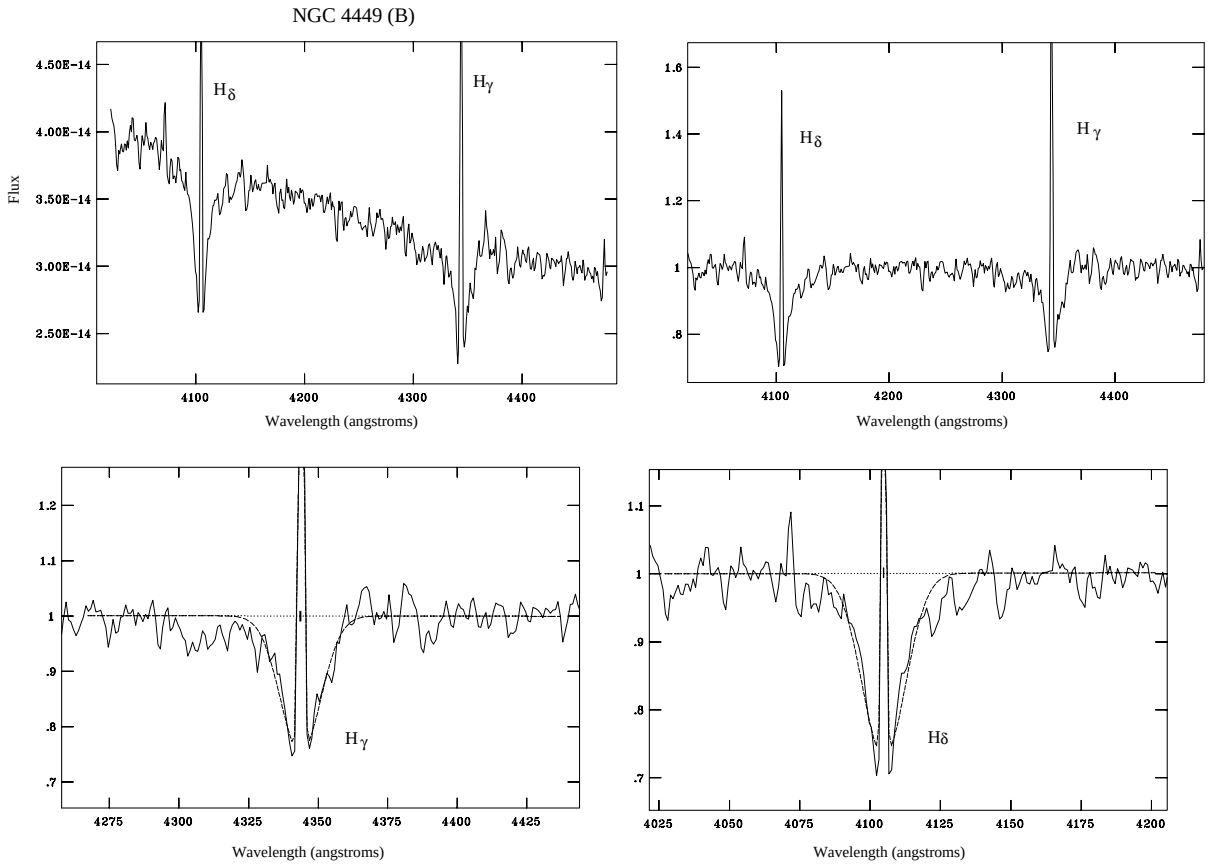

Fig. 11. NGC 4449 (B): *(top; from left to right)* absolute flux corrected spectrum; normalized spectrum; *(bottom)* respectively H_γ and H_δ lines with the Gaussian fit.

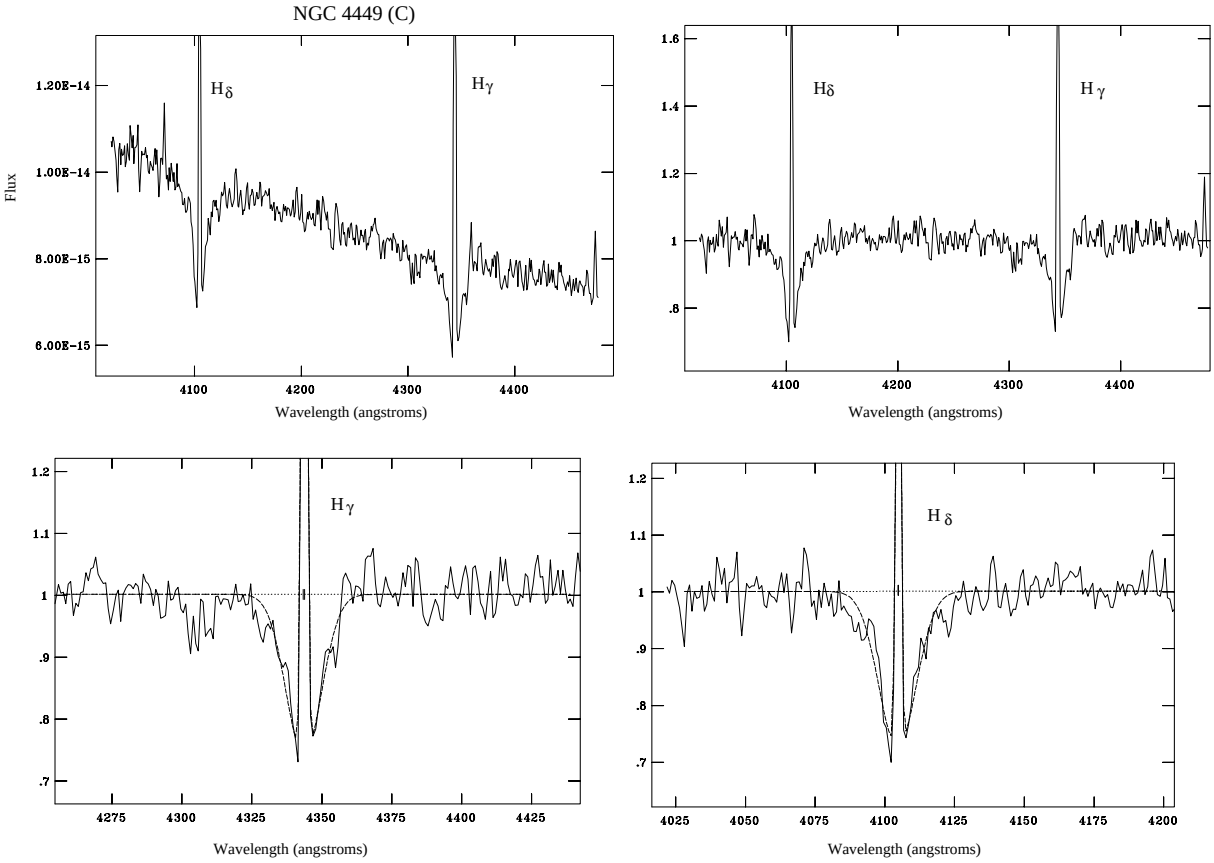

Fig. 12. NGC 4449 (C): *(top; from left to right)* absolute flux corrected spectra; normalized spectra; *(bottom)* respectively H_γ and H_δ lines with the Gaussian fit.

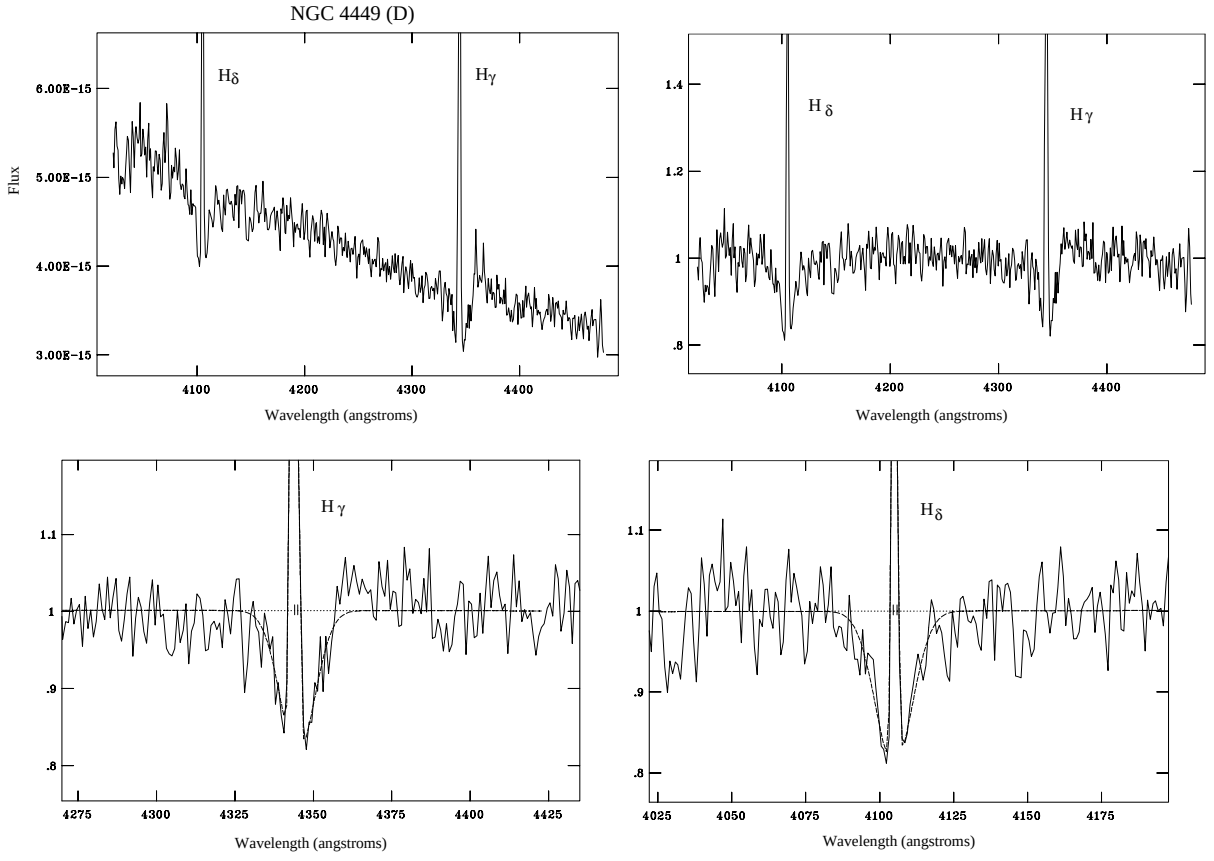

Fig. 13. NGC 4449 (D): *(top; from left to right)* absolute flux corrected spectrum; normalized spectrum; *(bottom)* respectively H_γ and H_δ lines with the Gaussian fit.

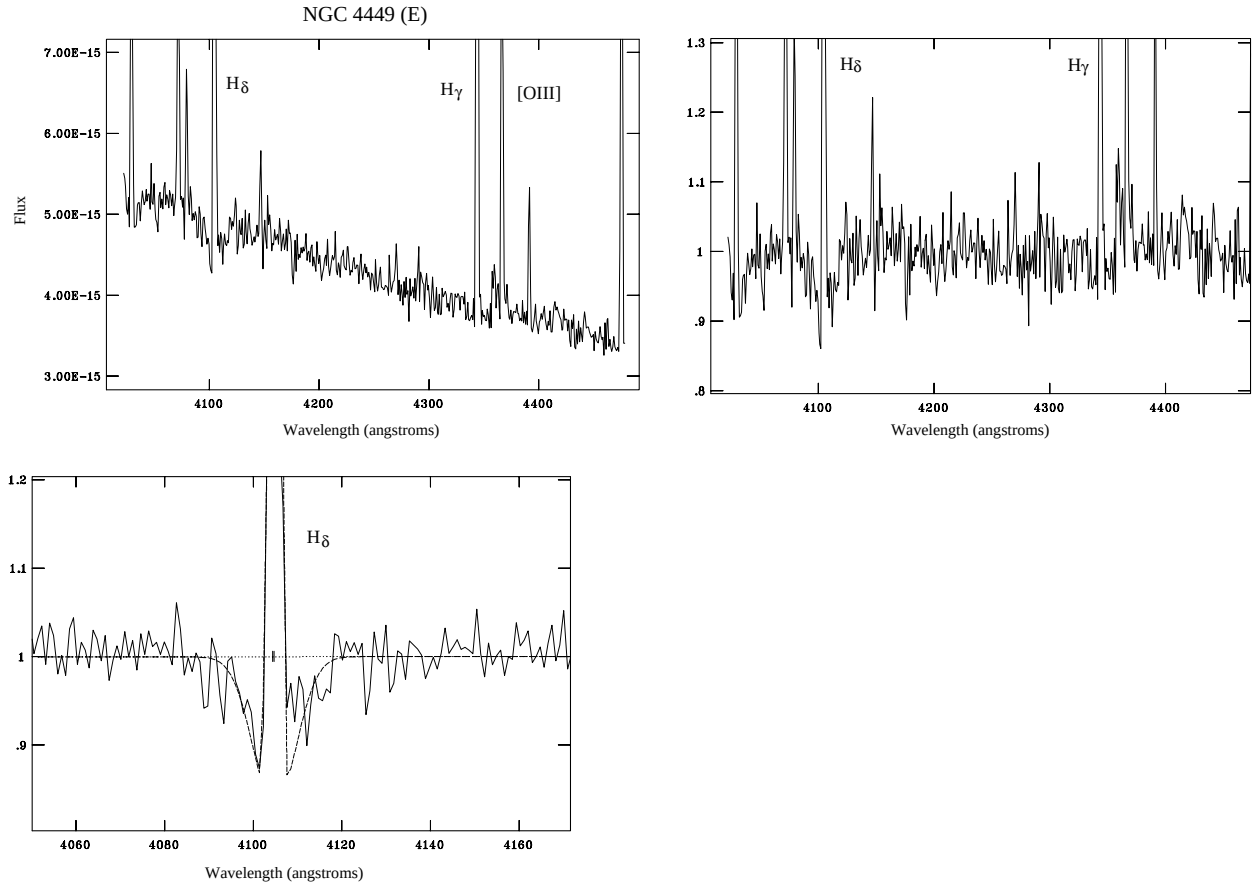

Fig. 14. NGC 4449 (E): *(top; from left to right)* absolute flux corrected spectrum; normalized spectrum; *(bottom)* H_δ line with the Gaussian fit.

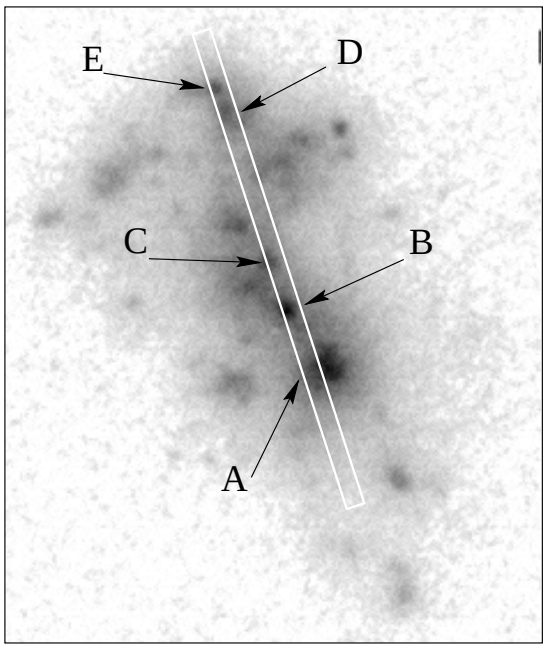

Fig. 15. NGC 4449: slit position and identification of the star forming regions.

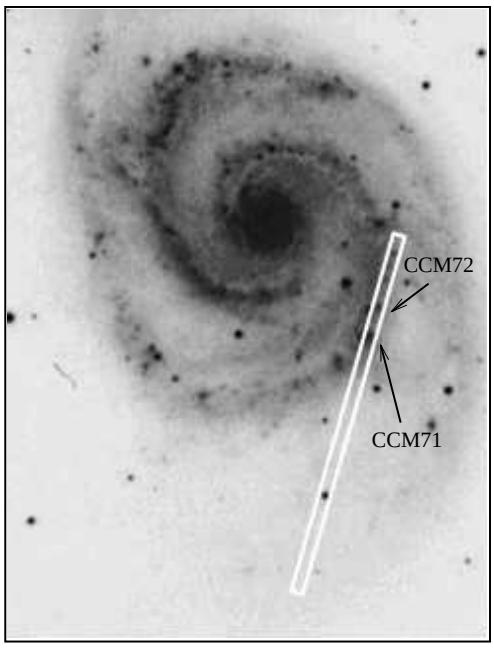

Fig. 16. M 51: slit position and identification of the star forming regions.

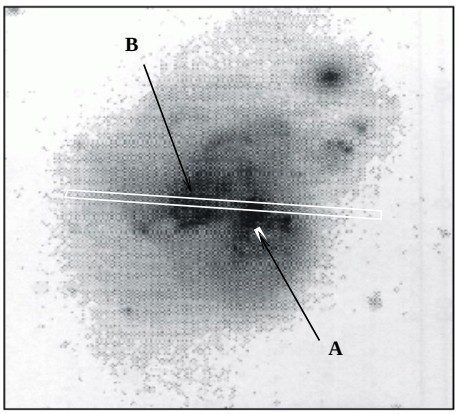

Fig. 17. Mrk 171: slit position and identification of the star forming regions.

of the stellar population and the IMF in the studied HII regions as well as for understanding the star–forming processes.

Acknowledgements. This work was partly supported by the Jumelage Astrophysique France-Arménie a bilateral program funded by Centre National de la Recherche Scientifique, the French Ministère des Affaires Étrangères and Ministère de la Recherche et de la Technologie. A. Sinanian and A. Petrosian thank the Institute d'Astrophysique de Paris for its hospitality during the periods this work was elaborated. We thank the referee F. Bresolin for his constructive comments.

References

Arnault, Ph., Kunth, D., & Schild, H. 1989, A&A, 224, 73
Augarde, R., & Lequeux, J. 1985, A&A, 147, 273
Boker, T., van der Marel, R. P., Mazzuca, L., et al. 2001, AJ, 121, 1473
Bresolin, F., & Kennicutt, R. C. 2002, ApJ, accepted [astro-ph/0202383]
Brocklehurst, M. 1971, MNRAS, 153, 471
Cananzi, K., Augarde, R., & Lequeux, J. 1993, A&AS, 101, 599
Carranza, G., Crillon, R., & Monnet, G. 1969, A&A, 1, 479
Copetti, M. V. F., Pastoriza, M. G., & Dottori, H. A. 1985, A&A, 152, 427
Crillon, R., & Monnet, G. 1969, A&A, 1, 449
Diaz, A. I., Terlevich, E., Vilchez, J. M., Pagel, B. E. J., & Edmunds, M. G. 1991, MNRAS, 253, 245
Gonzalez-Delgado, R. M., & Leitherer, C. 1999, ApJS, 125, 479
Gonzalez-Delgado, R. M., Leitherer, C., & Heckman, T. M. 1999, ApJS, 125, 489
Hill, R. S., Fanelli, M. N., Smith, D. A., et al. 1998, ApJ, 507, 179
Hodge, P. W. 1969, ApJS, 18, 73
Hodge, P. W., & Kennicutt, R. C. Jr. 1983, AJ, 88, 296
Holtzman, J. A., Mould, J. R., Gallagher, III J. S., et al. 1997, AJ, 113, 656
Hyland, A. R., Straw, S., Jones, T. J., & Gatley, I. 1992, MNRAS, 257, 391
Izotov, Y. I., Thuan, T. X., & Lipovetsky, V. A. 1997, ApJS, 108, 1
Jones, L. A., & Worthey, G. 1995, ApJ, 446, L31
Kennicutt, R. C. Jr. 1984, ApJ, 287, 116
Kewley, L. J., Dopita, M. A., Sutherland, R. S., Heisler, C. A., & Trevena, J. 2001, ApJ, 556, 121
Lemaître, G., Kolher, D., Lacroix, D., Meunier, J. P., & Vin, A. 1990, A&A, 228, 546
Lequeux, J., Maucherat-Joubert, M., Deharveng, M., & Kunth, D. 1981, A&A, 103, L305
Mas-Hesse, J. M., & Cerviño, M. 1994, A&A, 284, 749
Mas-Hesse, J. M., & Kunth, D. 1991, A&AS, 88, 399
Mas-Hesse, J. M., & Kunth, D. 1999, A&A, 349, 765
Massey, P., & Hunter, D. A. 1998, ApJ, 493, 180
Mazzarella, J. M., & Boroson, T. A. 1993, ApJS, 85, 27
McCall, M. L., Rybski, P. M., & Shields, G. A. 1985, ApJS, 57, 1
Moy, E., Rocca-Volmerange, B., & Fioc, M. 2001, A&A, 365, 347
Oey, M. S., & Massey, P. 1995, ApJ, 452, 210
Parker, J. W., Garmany, C. D., Massey, P., & Walborn, N. R. 1992, AJ, 103, 1205
Petrosian, A. R., & Burenkov, A. N. 1993, A&A, 279, 21
Rose, J. A. 1985, AJ, 90, 1927
Rose, J. A. 1994, AJ, 107, 206
Salzer, J. J. 1989, ApJ, 347, 152
Schaerer, D., & Vocca, W. D. 1998, ApJ, 497, 618
Shields, G. A., & Searle, L. 1978, ApJ, 222, 821
Sirianni, M., Nota, A., Leitherer, C., de Marchi, G., & Clampin, M. 2000, ApJ, 533, 203
Stasinska, G., Schaerer, D., & Leitherer, C. 2001, A&A, 370, 1
Torres-Peimbert, S., Peimbert, M., & Fierro, J. 1989, ApJ, 345, 186
Whitford, A. E. 1958, AJ, 63, 201
Worthey, G. 1996, in From Stars to Galaxies: The Impact of Stellar Physics on Galaxy Evolution, ed. C. Leitherer, U. Fritze-von Alvensleben, & J. Huchra (ASP: San Francisco), ASP Conf. Proc., 98, 467
Worthey, G., & Ottaviani, D. L. 1997, ApJS, 111, 377